A New Approach to Iris Pattern Recognition

Yingzi Du*, Robert Ives, Delores Etter, Thad Welch
Electrical Engineering Department
United States Naval Academy
Annapolis, MD 21402
*yingzidu@ieee.org; phone: 1 410 293-6158; fax: 1 410 293-3493

ABSTRACT

An iris identification algorithm is proposed based on adaptive thresholding. The iris images are processed fully in the spatial domain using the distinct features (patterns) of the iris. A simple adaptive thresholding method is used to segment these patterns from the rest of an iris image. This method could possibly be utilized for partial iris recognition since it relaxes the requirement of using a majority of the iris to produce an iris template to compare with the database. In addition, the simple thresholding scheme can improve the computational efficiency of the algorithm. Preliminary results have shown that the method is very effective. However, further testing and improvements are envisioned.

Keywords: Iris Identification, adaptive thresholding, iris pattern.

1. INTRODUCTION

The iris (Fig. 1) provides one of the most stable biometric signals for identification, with a distinctive texture that is formed before age one and remains constant throughout life unless there is an injury to the eye [1-2]. Compared with other biometric features such as face and fingerprint, iris patterns are more stable and reliable [1-2].

Current approaches to iris pattern recognition include: the 2-D Gabor wavelet approach by Daugman [3], the Laplacian parameter approach by Wildes *et al.* [4], zero-crossings of the 1-D wavelet transform at various resolution levels by Boles *et al.* [5], the Independent Component Analysis (ICA) approach by Huang *et al.* [6], the texture analysis using multi-channel Gabor filtering and wavelet transform by Zhu *et al.* [7], the circular symmetric filter approach by Ma *et al.* [8], the self-organizing neural network approach by Liam *et al.* [9], and the one-dimensional approach by Du *et al.* [10]. Each method has its own advantages and disadvantages. Among them,

Daugman's 2-D Gabor wavelet approach has been successfully tested using a large scale iris database and has been commercialized by Iridian [11], and the one-dimensional approach has been tested for use with partial iris identification [12].

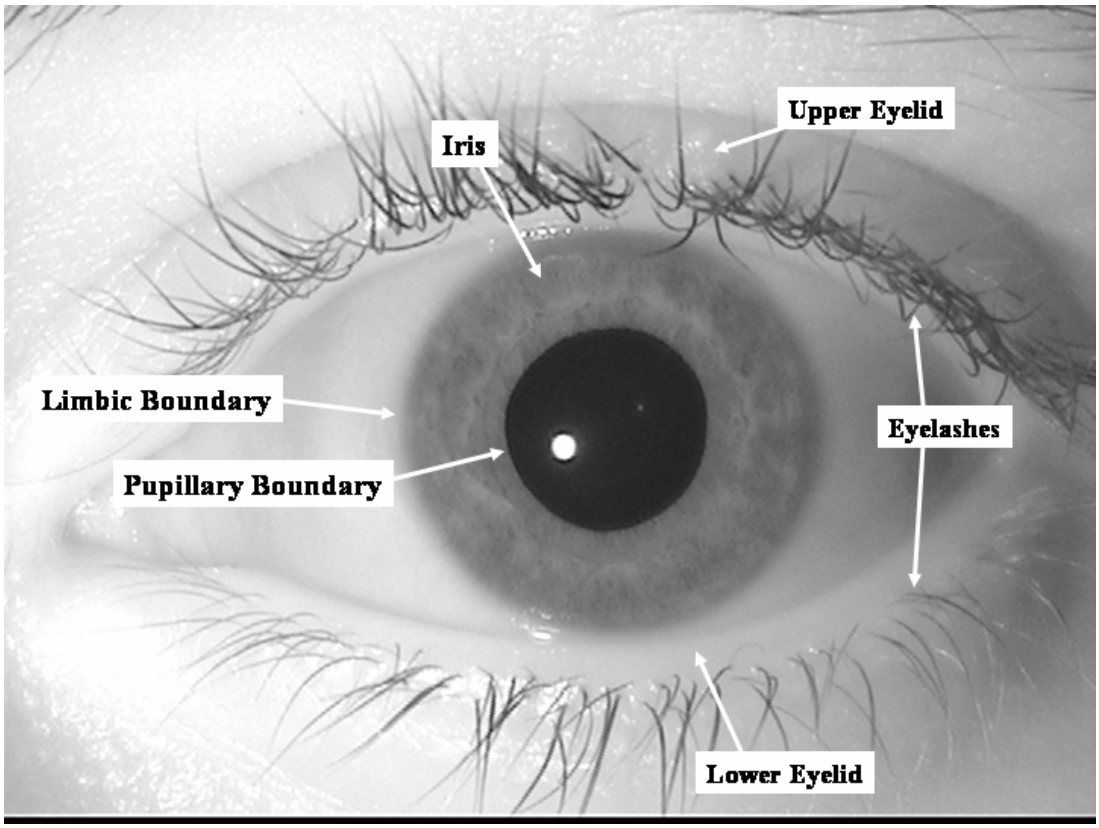

Figure 1: An iris image.

In this paper, a new iris recognition approach is proposed. Section 2 introduces and describes the adaptive thresholding algorithm used in enhancing templates. Section 3 proposes the new iris recognition approach based on the adaptive thresholding algorithm. Section 4 presents experimental results, and Section 5 draws conclusions.

2. Adaptive Image Thresholding

Image thresholding segments an image into a binary image by setting all pixels whose intensity values are above a certain threshold to "1" and all the remaining pixels to "0". The conventional thresholding operator uses a global threshold for all pixels [13-15]. Adaptive thresholding changes the threshold dynamically over the image, and can adapt to illumination and contrast changes [16]. A simple approach to adaptive image thresholding is to use a local threshold, which statistically

examines the intensity values of the local neighborhood of each pixel. The statistic which is most appropriate in computing the threshold depends largely on the input image. Based on our experimental results, we used the mean of the local intensity distribution in a fixed overlapping window, with the threshold chosen to be a constant value C less than the local mean: $T = mean\text{-}C$.

Choosing the size of the window for use with an iris image is very important. It must be large enough to cover a sufficient neighborhood, yet if chosen too large it can overlook important local variations. Fig. 2 shows an example of adaptive thresholding of a text image. Fig. 2(a) is a document with non-uniform illumination. Fig. 2(b) is the thresholding result using a global threshold, which produces a very poor result. Fig. 2(c) is the threshold result using adaptive thresholding with a 140×140 window and $C = 8$.

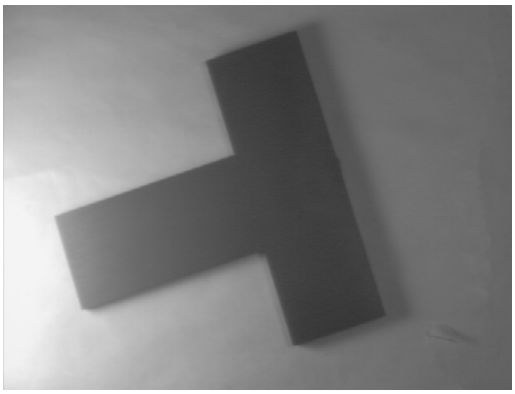

(a) Original gray-scale image

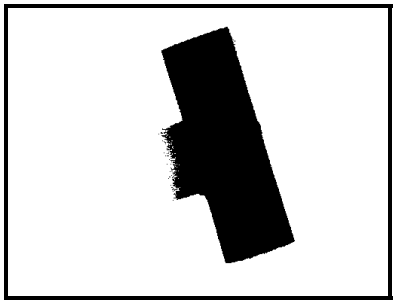

(b) Global thresholding result

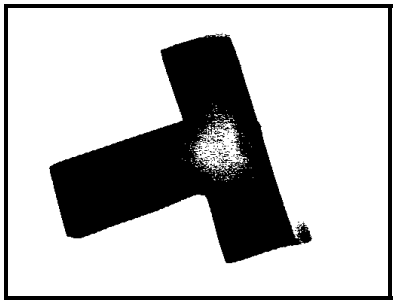

(c) Adaptive thresholding: C=8, window 140×140

Figure 2. An example of adaptive thresholding [17].

3. Iris Recognition System Architecture

The block diagram in Fig. 3 depicts the principle steps of the proposed iris recognition system, and is described in the following. The system has two sub–systems: the iris enrollment system and the iris identification system. The iris enrollment system (Fig. 3(a)) is to enroll the iris in the

database for further identification. The iris identification system (Fig. 3(b)) compares a newly input iris with the known irises in the database and decides if it is in the database.

The iris enrollment system (Fig. 3(a)) is comprised of the following modules: the Preprocessing Module, the Establish Coordinate System Module, the Mask Generation Module, the Adaptive Thresholding Module, the Iris Pattern Generation Module, the Enrollment Module, and the Iris Pattern Database. The iris identification system does not have the Enrollment Module, but has two additional modules: the Hamming Distance Module and the Identification Module.

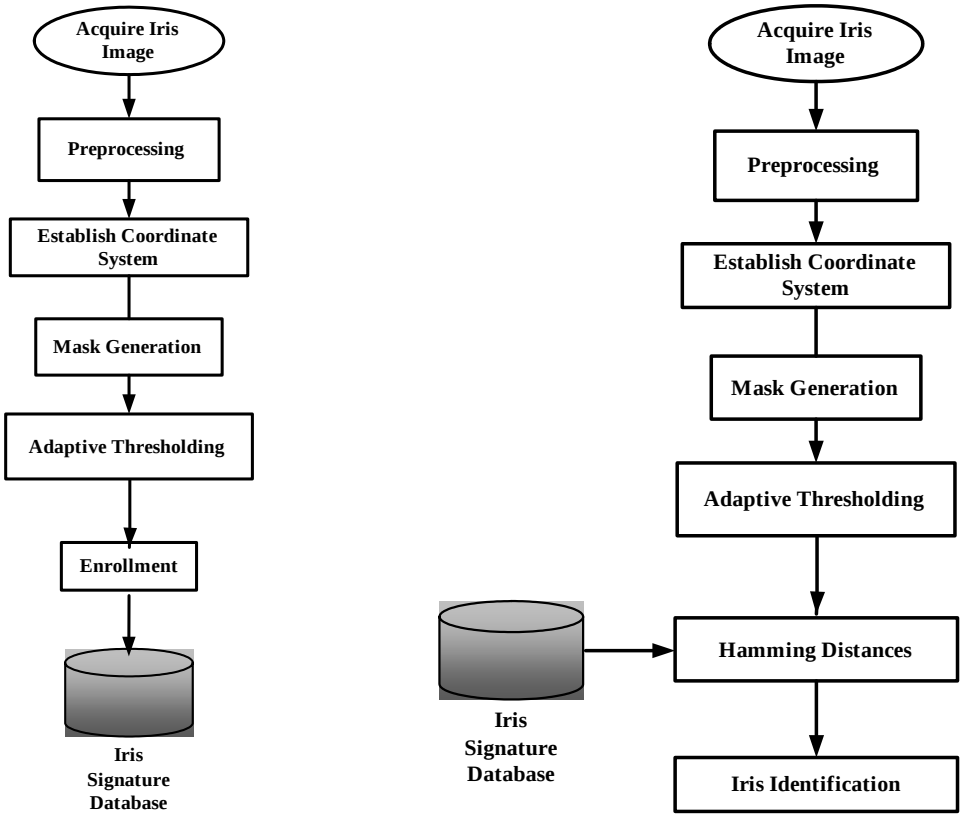

(a) Enrollment System (b) Identification System

Figure 3. Iris recognition system

3.1 Preprocessing Module

The Preprocessing Module locates the various components of the iris boundary. In particular, we find the limbic (outer) boundary of the iris, the pupillary (inner) boundary of the iris, and the

eyelids. As the first step, we discard every other row and column of the original iris image to reduce it (Fig. 4(a)) to ¼ of the original size to speed up the processing (Fig. 4(b)). The Canny method [18] was applied to this image for edge detection. The edge image was then thresholded and is shown in Fig. 4(c). There is a clear circle in the edge image in this figure that represents the outer edge of the pupil. The edges above and below the circle are the edges of eyelids and eyelashes. The circle parameters (center (x_0, y_0) and radius r_0) are then estimated and optimized for the pupillary boundary.

To remove the effects of eyelashes or high reflectance pixels (glare), a determination is made if any pixel value in the image is an outlier. To do this, we use edge detection to find the eyelids and eyelashes, and then mask them out.

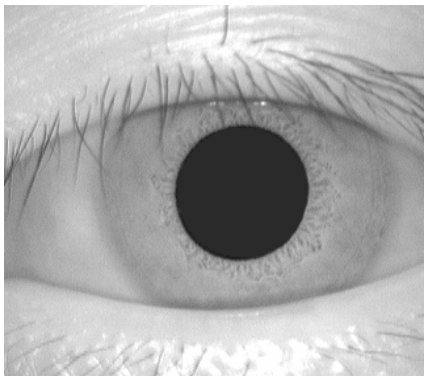

(a) Original iris image

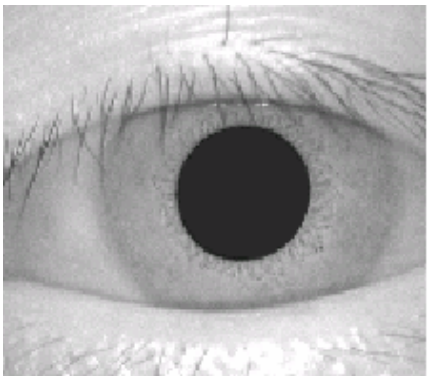

(b) ¼ size iris image

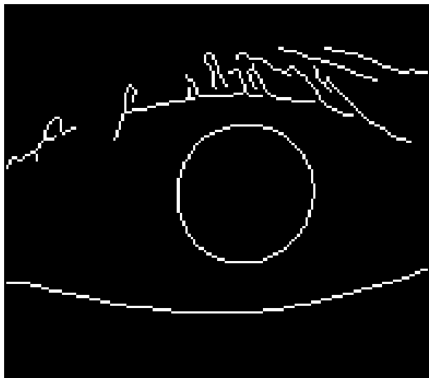

(c) Edges of the iris image

Figure 4. Iris Image Preprocessing

3.2. Establish Coordinate System

After preprocessing, the entire image is then transformed to polar coordinates (Fig, 5(a)) with center (x_0, y_0). On the polar axis, the limbic boundary is very nearly horizontal. Fig. 5 shows the iris image transformed into polar coordinates. A horizontal Sobel filter [16] is applied to detect the horizontal edges. The longest horizontal edge after the pupillary boundary is the limbic boundary (Fig. 5(b)). At this point, the inner and outer boundary of the iris have been determined. The next step is normalization.

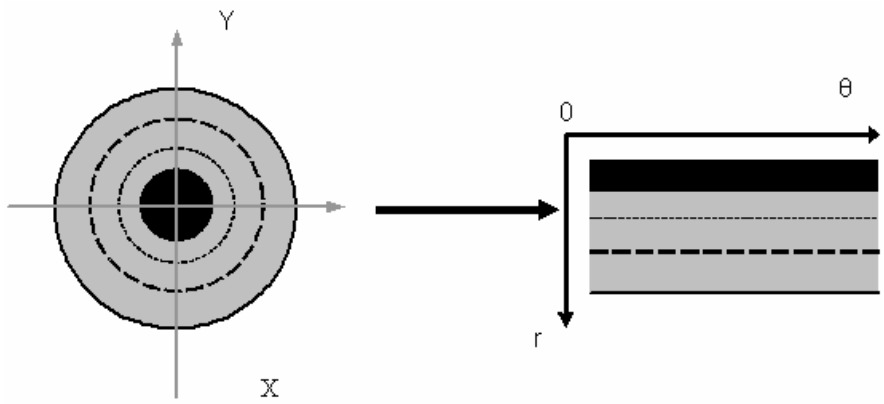

(a) Rectangular to polar transformation [1].

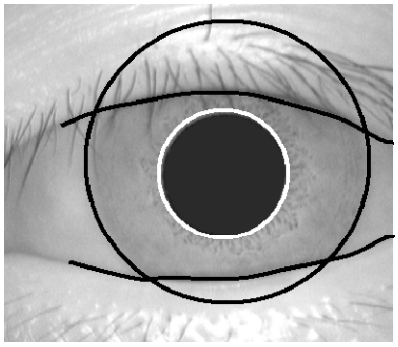

(d) After boundary detection

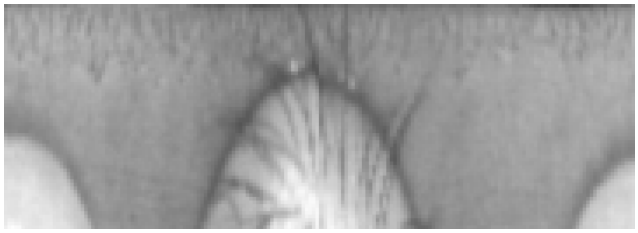

(c) Iris image in polar coordinates

Figure 5. Transformation of the iris image to polar coordinates.

3.3 Mask Generation Module

The size of the same iris taken at different times may be variable in the image as a result of changes in the camera-to-face distance [4,10]. Due to stimulation by light or for other reasons the pupil may be constricted or dilated. These factors will change the iris resolution, and the actual distance between the pupillary and the limbic boundary.

To solve these problems, the iris image is processed to ensure the accurate location of the virtual circle and to fix the resolution [10]. We normalize the distance between the pupillary and limbic boundary to be a constant $\tilde{L}$ pixels for all iris images. The value of $\tilde{L}$ should be decided based on the overall resolution of the iris images in the database. In our experiments, the iris images are all 280-by-320 pixels in dimension. The distance from the pupil to the limbic boundary usually fell in the range of 55~70 pixels. In this case, $\tilde{L}$ should be some value between 55 and 70, because it would be easier to shrink the image size via averaging pixel values than to enlarge the image via interpolating the pixels (which may introduce false patterns). In our case, we select $\tilde{L}$=56.

The iris area is then transformed using resolution invariant polar coordinates (which are different from the standard polar coordinates used in Section 3.2) to address the potential iris size difference [15]. For each pixel in the original iris image located at rectangular coordinates (x_i, y_i), we compute its polar coordinates (r_i,θ_i) as:

$$r_i = \frac{\tilde{L}}{L}\left(\sqrt{(x_i - x_0)^2 + (y_i - y_0)^2} - r_0\right), \qquad \theta_i = \begin{cases} \arcsin\left(\dfrac{y_i - y_0}{x_i - x_0}\right) & y_i \geq y_0 \\ \pi + \arcsin\left(\dfrac{y_i - y_0}{x_i - x_0}\right) & y_i < y_0 \end{cases}. \tag{1}$$

Here, (x_0, y_0) is the center of the pupil, and r_0 is the pupil's radius. L is the actual distance between the pupillary and limbic boundary in the original image. This step normalizes the radius of the limbic boundary to $\tilde{L}$ pixels.

At the same time, the boundary positions are transferred to the resolution invariant polar coordinates. The eyelids, eyelashes are marked "0" after being identified in the preprocessing module (see Fig. 4(C)). Fig. 6(a) shows the generated iris mask, where white represents the locations of iris pattern areas, and black represents the non-iris pattern areas, such as pupil pixels, eyelids, and eyelashes. Fig. 6(b) shows the resulting iris pattern after applying the mask. Note that the mask is resolution (scale) invariant.

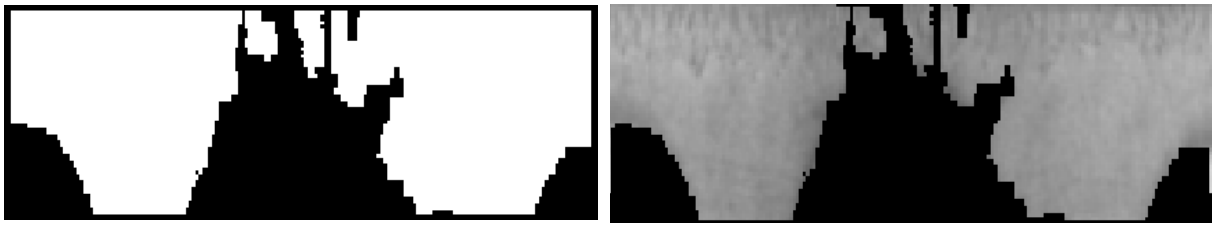

(a) The resolution invariant mask (b) The resolution invariant iris patterns

Figure 6. Iris Mask and Iris Patterns.

3.4. Adaptive Thresholding

To threshold the iris image to a binary image, the adaptive thresholding method introduced in Section 2 is used. It is applied only to those pixels identified in Section 3.3 as being actual iris pixels (that is, those pixels falling within the white area of Fig. 6(a)). The window size of the adaptive thresholding is 7×7 with $C = 3$. The value of C was chosen based on experimental results. Fig. 7 displays the adaptive thresholding applied to the image of Fig. 6(b): black areas are non-iris pixels, gray areas are pixels whose value fell at or below the adaptive threshold and white areas are pixels that fell above the adaptive threshold.

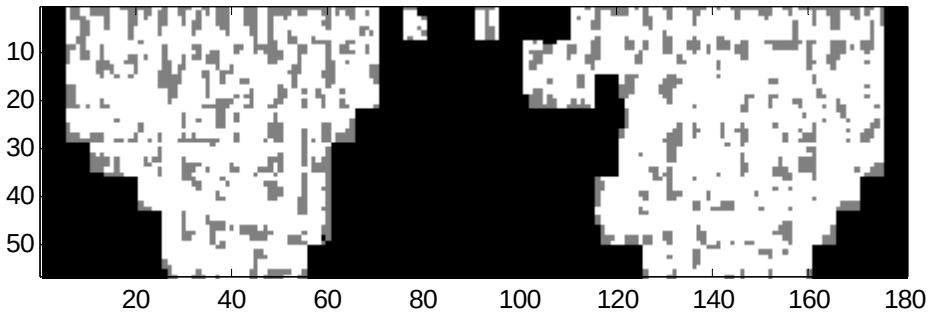

Figure 7. Adaptive thresholding result. White (‘2’) represents pixels with value above the adaptive threshold, gray (‘1’) are pixels with value below the threshold, and black (‘0’) are non-iris pixels.

3.5. Enrollment Module

This module is only in the iris enrollment system. For an iris pattern to be recognizable in the system, we first need to enroll it in the database. Enrollment usually takes multiple iris images of the same iris to register and generate the enrollment iris signature[10]. Here, our system uses four iris images for enrollment. First, we separate the for iris images into two groups of two images

each. After generating iris patterns for each iris image, Eq. 2 is applied to each group to generate a new iris pattern, which is the representative pattern of each group. The enrolled iris signature is generated by applying the same equation to these two representative patterns.

$$P_new = \begin{cases} 2 & \text{if } P_1 = 2 \ \& \ P_2 = 2 \\ 1 & \text{if } P_1 = 1 \ \& \ P_2 = 1 \\ 0 & \text{if } (P_1 = 0 \ \& \ P_2 = 0) \text{ or } (P_1 = 1 \ \& \ P_2 = 2) \text{ or } (P_1 = 2 \ \& \ P_2 = 1) \\ P_1 & \text{if } P_1 > 0 \ \& \ P_2 = 0 \\ P_2 & \text{if } P_1 = 0 \ \& \ P_2 > 0 \end{cases} \tag{2}$$

where P_1 and P_2 are iris patterns of iris images in the group. The P_new is the newly generated iris pattern.

3.6. Iris Signature Database

Enrolled iris patterns are processed to form their iris signature, then stored in the Iris Signature Database.

3.7. Iris Matching Module

This module is only in the iris identification system. When an iris image is presented for identification, its iris signature is generated, and we attempt to match it with the enrolled iris signatures in the database via circular convolution. The matching score is based on the Hamming distance. The calculation of the Hamming distance is:

$$d = \frac{\| (P \otimes S) \cap M_p \cap M_S \|}{\| M_p \cap M_S \|} . \tag{3}$$

Here, P represents the enrolled signatures, S represents the input iris signature, M_p and M_S are the enrolled and input signal masks, and $M_S = (S > 0)$ and $M_S = (P > 0)$ (i.e., M_s and M_p determine the locations of iris pixels in each mask). The output of this module is the identification result.

3.8 Iris Identification Module

This module is only in the iris identification system. Based on the Hamming distance generated in 3.7, the Identification Module will generate either "1"—indicating a match (if d >0.8) or "0"—indicating no match (if $d \leq 0.8$).

4. EXPERIMENTAL RESULTS

The CASIA database [19] was used to test our algorithm, which include 756 iris images from 108 different eyes (7 iris images of each eye). Four eyes could not be enrolled, due to low quality or iris obscuration. Fig. 8 shows an example of an iris image that could not be enrolled, due to the long eyelashes covering the iris. This means that in our iris database, we have 104 different iris signatures

756 iris images were used to test the accuracy rate and the False Acceptance Rate (FAR). The definition of the Accuracy rate and the FAR [20] are:

$$Accuracy(\%) = \frac{\text{number of images of correctly identificated}}{\text{total number of images identified}} \times 100\% \tag{4}$$

$$FAR(\%) = \frac{\text{number of incidents of false acceptance}}{\text{total number of images accepted}} \times 100\% \tag{5}$$

All the images identified were correct, achieving a 100% accuracy rate. There were no false acceptances (0% FAR). However, the system could not identify 46 iris images; this area requires future evaluation.

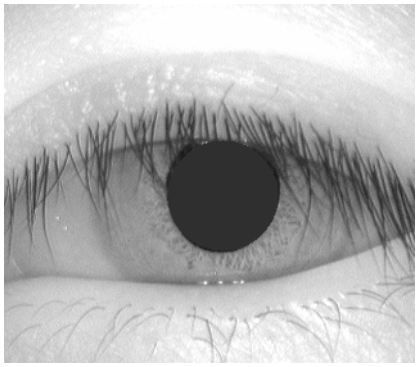

Figure 8. An example of a noisy iris image

5. CONCLUSIONS

We have proposed a simple approach to generate an iris signature, which is based on the adaptive image thresholding. This method uses spatial processing, and local neighborhoods to generate the threshold. This method can potentially be used for partial iris recognition since it relaxes the requirement of using a majority of the iris to generate the signature. In addition, the simple thresholding scheme can improve the efficiency of the algorithm. The preliminary research results have shown that the method is very effective. However, there are four iris images that cannot be enrolled in this system, and 46 iris images that cannot be identified; some areas of improvement are noted.

ACKNOWLEDGEMENTS

Portions of the research in this paper use the CASIA iris image database [19] collected by Institute of Automation, Chinese Academy of Sciences. This work has been sponsored in part by the U.S. National Security Agency.

REFERENCES

[1] Y. Du, R. W. Ives, and D. M. Etter, "Iris Recognition", *The Electrical Engineering Handbook*, 3rd Edition, Boca Raton, FL: CRC Press, 2004 (in press).

[2] Woodward, N.M. Orlans, and P.T. Higgins, *Biometrics*, The McGraw-Hill Company, Berkeley, California, 2002.

[3] J. Daugman, "High Confidence Visual Recognition of Persons by a Test of Statistical Independence", *Pattern Analysis and Machine Intelligence, IEEE Transaction on*, Vol. 15, No. 11, 1148-1161, 1993.

[4] R.P. Wildes, J.C. Asmuth, G.L. Green, S.C. Hsu, R.J. Kolczynski, J.R. Matey, and S.E. McBride, "A Machine Vision System for Iris Recognition", Mach. Vision Application, Vol. 9, pp.1-8, 1996.

[5] W.W. Boles and B. Boashash, "A Human Identification Technique Using Images of the Iris and Wavelet Transform", Signal Processing, IEEE Transactions on, Vol. 46, No. 4, 1998.

[6] Y.-P. Huang, S.-W. Luo, E.-Y. Chen, "An Efficient Iris Recognition System", Proceedings of the First International Conference on Machine Learning and Cybernetics, pp. 450-454, 2002.

[7] Y. Zhu, T. Tan, and Y. Wnag, "Biometric Personal Identification Based on Iris Patterns", Pattern Recognition, 15th International Conference on , Vol. 2 , pp. 801 –804, 2000.

[8] L. Ma, Y. Wang, and T. Tan, “Iris Recognition Using Circular Symmetric Filters”, Pattern Recognition, 16th International Conference on , Vol. 2 , pp. 414-417, 2002 .

[9] L.W. Liam, A. Chekima, L.C. Fan, and J.A. Dargham, “Iris Recognition Using Self-Organizing Neural Network”, Student Conference on Research and Development Proceedings, pp. 169-172, 2002.

[10] Y. Du, R. W. Ives, D. M. Etter, T. B. Welch, and C.-I Chang, "A One Dimensional Approach to Iris Recognition", Proceedings of SPIE Volume 5404, Biometric Technology for Human Identification, pp. 237-247, Apr., 2004.

[11] http://www.iridiantech.com/, (2004).

[12] Y. Du, B. Bonney, R. W. Ives, D. M. Etter, and R. Shcultz, “Partial Iris Recognition Using a 1-D Approach: Statistics and Analysis”, submitted to IEEE International Conference on Acoustics, Speech, and Signal Processing (ICASSP), 2005.

[13] N. Otsu, "A threshold selection method from gray-level histograms," *IEEE Trans. System Man Cybernetics*, Vol. SMC-9, No. 1, pp. 62-66, 1979.

[14] J. Wang, Y. Du, C.-I Chang and P. Thouin, "Relative Entropy-Based Methods for Image Thresholding," *International Symposium. Circuit and Systems (ISCAS) 2002*, 26-29 May, Scottsdale, Arizona, 2002.

[15] Y. Du, C.-I Chang, and P.D. Thouin, "An Unsupervised Approach to Color Video Thresholding", *Optical Engineering*, Vol. 43, No. 2, 282-289, 2004.

[16] R. C. Gonzalez, R. E. Woods, Digital Image Processing, 2nd Edition, Upper Saddle River, NY: Prentice Hall, 2002.

[17] http://www.cee.hw.ac.uk/hipr/html/adpthrsh.html

[18] R.C. Gonzales and R.E. Woods, Digital Image Processing, Second Edition, Prentice Hall, New Jersey, 2001

[19] CASIA Iris Image Database, http://www.sinobiometrics.com

[20] R. W. Ives, and D. M. Etter, “Introduction to Biometrics”, *The Electrical Engineering Handbook*, 3rd Edition, Boca Raton, FL: CRC Press, 2004 (in press).